Electronic Supplementary Information (ESI) for:

Singular behaviour of atomic ordering in Pt–Co nanocubes starting from core–shell configurations

Kohei Aso,*[a] Hirokazu Kobayashi,[b] Shotaro Yoshimaru,[c] Xuan Quy Tran,[d]

Miho Yamauchi,[c,e] Syo Matsumura,[d,f] and Yoshifumi Oshima[a]

[a] School of Materials Science, Japan Advanced Institute of Science and Technology, 1-1 Asahidai, Nomi, Ishikawa 923-1292, Japan

[b] Division of Chemistry, Graduate School of Science, Kyoto University, Kitashirakawa Oiwake-cho, Sakyo-ku, Kyoto 606-8502, Japan

[c] Department of Chemistry, Faculty of Science, Kyushu University, 744 Moto-oka, Nishi-ku, Fukuoka 819-0395, Japan

[d] Department of Applied Quantum Physics and Nuclear Engineering, Graduate School of Engineering, Kyushu University, Moto-oka 744, Nishi-ku, Fukuoka 819-0395, Japan

[e] International Institute for Carbon-Neutral Energy Research (WPI-I2CNER), Kyushu University, 744 Moto-oka, Nishi-ku, Fukuoka 819-0395, Japan

[f] The Ultramicroscopy Research Center, Kyushu University, Moto-oka 744, Nishi-ku, Fukuoka, 819-0395, Japan

* Corresponding author's e-mail: aso@jaist.ac.jp

Chemical synthesis of as-grown nanoparticles

Platinum@Cobalt (Pt@Co) nanoparticles were prepared by a chemical synthesis proposed by Choi et $al.$[1] A mixture of $Pt(acac)_2$ (25 mg, 0.064 mmol) and $Co_2(CO)_8$ (5.4 mg, 0.016 mmol) was prepared in a heat resistant glass vial, and then 1,2-Hexadecanediol (15 mg), benzyl ether (4 mL), oleylamine (4 mL), and oleic acid (0.5 mL) were added. The slurry was heated at 200°C

for 180 min with a temperature increase rate of 2–3°C/min under an air atmosphere. After centrifugation at 7000 rpm for 10 min, the supernatant was removed, and hexane was added to disperse the synthesized particles. Fig. S1 shows a low magnification image acquired by scanning transmission electron microscopy (STEM).

Consideration of the annealing experiments

To obtain an atomic-resolution image in STEM, the nanoparticle should be aligned along [100] crystal orientation. The angle alignment is conducted by tilting a sample holder for the angle range of ±15˚. The heating holder has a highly limited tilt range of ~±5˚ to avoid hitting the electromagnetic lens in STEM. This is because the holder has a heater at the sample position and is thicker than a usual holder. This prevents us to observe the atomic-resolution imaging in *in-situ* STEM experiments. Therefore, we choose pre-annealing and *ex-situ* experiments for STEM observations. After being annealed, the nanoparticles are observed by using a high-angle double tilt holder (EM-01040RSTHB, JEOL, Japan). For this holder, the tilting angle is in the range of ~±25˚ around the holder axis and ~±25˚ along the vertical axis. *In-situ* experiments were only conducted in a conventional TEM without tilting the heating holder.

Preparation of initial and pre-annealed samples

A carbon film with a Molybdenum (Mo) grid (STEM Co., Ltd., Japan) was used to support the particles. Before mounting the particles, the Mo grid was baked in a vacuum (~1×10^{-5} Pa) at the temperature of 900 ˚C for 120 min to avoid contamination during heating experiments. After baked out, a carbon support film was deposited onto the grid. The nanoparticle solution was dropped onto the grid, and then the grid was dried in a desiccator (~1×10^{2} Pa). The annealed samples were prepared by heating the sample grids on a heating holder EM-31670SHTH (JEOL, Japan) and 652 (Gatan, US).

High-angle annular dark-field (HAADF) imaging

The HAADF observations were carried out using scanning TEM (STEM) of JEM-ARM200F (JEOL, Japan) with a spherical aberration corrector. The acceleration voltage of an electron beam was set to be 200 kV. The convergence semi-angle of the incident electron probe was 20 mrad. The observations were conducted with a fast scan speed of an electron probe to suppress the disturbance influence of image distortion (due to the sample drift) and noise.[2,3] A series of HAADF images were acquired for an area of interest with a dwell time as short as 1 μs/pixel with an image size of 1024 pixels × 1024 pixels. After positional alignment of the image series with 10–30 frames, the series was integrated to construct the final image. To compare with the atomic arrangements in the experimental images, the atomic models were visualized by the software VESTA[4] in Main Fig. 2.

Energy-dispersive X-ray spectroscopy (EDS) analysis

The EDS analysis was performed using another STEM, JEM-ARM200CF (JEOL, Japan), equipped with two silicon drift detectors for characteristic X-ray detection. The acceleration voltage was set to be 200 kV. The convergence semi-angle was 20 mrad. A software NSS (Thermo Fisher Scientific Inc., US) was used for the quantification of the elements.

Raw EDS data were denoised by block matching 3D (BM3D) filtering.[5] The BM3D processing was repeated to properly denoise EDS maps including only up to several counts per pixel.[6] Python programming code was used to carry out the procedures. Further details of BM3D filtering of EDS data will be described somewhere appropriate.

***In-situ* heating electron diffraction experiments**

In-situ TEM heating experiments were conducted for as-grown Pt@Co core–shell nanoparticles with an annealing temperature of 700°C for 3 hours, at the rate of ~0.6°C / sec, under the vacuum (~1×10^{-4} Pa). The observations were performed in JEM-3200FSK (JEOL,

Japan) with an acceleration voltage of 300 kV.

Fig. S8 shows the bright-field images and selected area electron diffraction (SAED) patterns, before and after annealing. Before annealing, the SAED pattern of the corresponding region show only fcc rings. Contrary, additional rings are shown in the SAED pattern after the annealing. The additional rings were explained by the ordered structure, as indicated in Fig. S8. Here, both $L1_0$ and $L1_2$ structures can induce the additional diffraction rings. Only the $L1_0$ structure induces the splitting of some rings due to tetragonal distortion (*e.g.*, 200 and 002), but the tetragonality (c/a) is too small to observe the split rings.

To confirm the structure type, we performed HAADF observations of the particles after the *in-situ* annealing experiment. Figs. S9a and b are the obtained images. The particles mainly consist of the A1 core and $L1_0$ shells. In some areas in Fig. S9a and b, $L1_2$-like contrast can be seen with the size of ~1–2 nm, especially around the interface between the A1 core and $L1_0$ shell. The $L1_2$–Pt_3Co structure indicates that the interface is Pt-rich, suggesting the Pt atoms diffused from the core to the shell.

Ex-situ tracking of the same particle before and after being annealed

To observe the same particle before and after being annealed, we have tried *ex-situ* experiments with the following three steps. First, initial nanoparticles were mounted on the two-axis tilting holder. The nanoparticles were observed in atomic resolution, and their positions were carefully recorded by acquiring several low-resolution images (Fig. S5 left). Second, the grid was transferred onto the heating holder and then annealed (at 700 ˚C for 3 hours with a cooling rate of −0.6°C/sec). Finally, the annealed grid was again mounted on the tilting holder. We again observed the same particles after being annealed (Fig. S5 right).

The results are summarised in Fig. S6. The initial nanoparticles (Fig. S6a–e) had similar morphology and structure to the particle shown in Fig. 2a Main. After being annealed, the

particles changed their structure into $L1_0$ multidomain (Fig. S6a'–e'), which are similar to the particle in Fig. 2c Main.

Other annealed particles

Other particles, that were annealed at 700 ˚C for 3 hours with a cooling rate of −0.6°C/sec, are shown in Figs. S7 and S9c–d. The particles in Fig. S7 were observed from the annealed samples used for *ex-situ* observations in Fig. S6. The particles in Fig. S9c–d were observed from the annealed samples used for another *in-situ* experiment in the conventional TEM. These particles also show the $L1_0$ multidomain structure, which is similar to the particle shown in Fig. 2c of Main.

Atomic distance analysis of $L1_0$ domains

The bulk $L1_0$ structure is known to contain the tetragonality c/a of 0.973 [7]. To investigate the tetragonality of multidomain nanoparticles, we analysed the atomic distance from the HAADF image in Main Fig. 2c.

The analysis procedure is as follows. First, we fitted Gaussian distribution functions to the HAADF image to obtain the positions of atomic columns[2,3,8]. Second, domain regions were defined (Fig. S3a): Domain 0 is the reference core area for the following step, and Domains 1–4 are the $L1_0$ domains. Third, we corrected an image distortion due to the sample drift and STEM equipment[9]. Here, we simply assumed that Domain 0 reflects the A1-Pt core, and the affine transformation was applied such that Domain 0 has a perfect square lattice. Fourth, we obtained the distances a and c for a given atomic position (Fig. S3b). Finally, we calculated the tetragonality.

Fig. S3c shows the obtained plot of the tetragonality. Domain 0 has the perfect square lattice due to the assumption above. Domains 1–4 have a tetragonality of 0.96–0.97, which correspond to the reported balk value. This result supports our conclusion that the domains have the $L1_0$

structure from the viewpoint of tetragonality.

Calculation of diffusion lengths

The diffusion lengths were calculated by using Main Eq. 1 with the diffusion coefficient D_0 (m²/sec) and activation energy Q (eV) summarised in Table S1 below. Main Fig. 4 was plotted from the calculation on the Pt–iron (Pt–Fe) interdiffusion in alloys disordered PtFe,[10] $L1_0$–PtFe along c–axis,[10] and $L1_2$–Pt$_3$Fe.[11] As described in Main, the Pt–Fe system was used for the ordered structures because the Pt–Co system has not been studied to the best of our knowledge. The rationality to use the Pt–Fe system was evaluated by comparing relating systems of Pt, Co, and Fe. We compared the diffusion of tracer atoms in the other types of atoms (tracer diffusion).[12] We also compared the diffusion where the two types of atoms move each other (interdiffusion).[10,13] As shown in Fig. S11, the diffusion lengths do not vary largely for the Pt–Co and Pt–Fe systems, compared to much shorter diffusion lengths in ordered structures (Main Fig. 4).

Supplementary Table

Table S1 Pre-exponential term D_0 of diffusion constant and activation energy Q

	D_0 [m²/sec]	Q [eV]
PtFe (disordered) [10]	4.2×10^{-4}	3.08
L1$_2$–Pt$_3$Fe [11]	1.9×10^{-5}	3.04
L1$_0$–PtFe // c-axis [10]	7.6×10^{-2}	3.80
Pt diffusion in Co [12]	6.5×10^{-5}	2.89
Co diffusion in Pt [12]	2.0×10^{-3}	3.22
Pt diffusion in Fe [12]	1.2×10^{-4}	2.95
Fe diffusion in Pt [12]	2.5×10^{-6}	2.52
PtCo (disordered) [13]	6.4×10^{-5}	2.84

Supplementary Figures
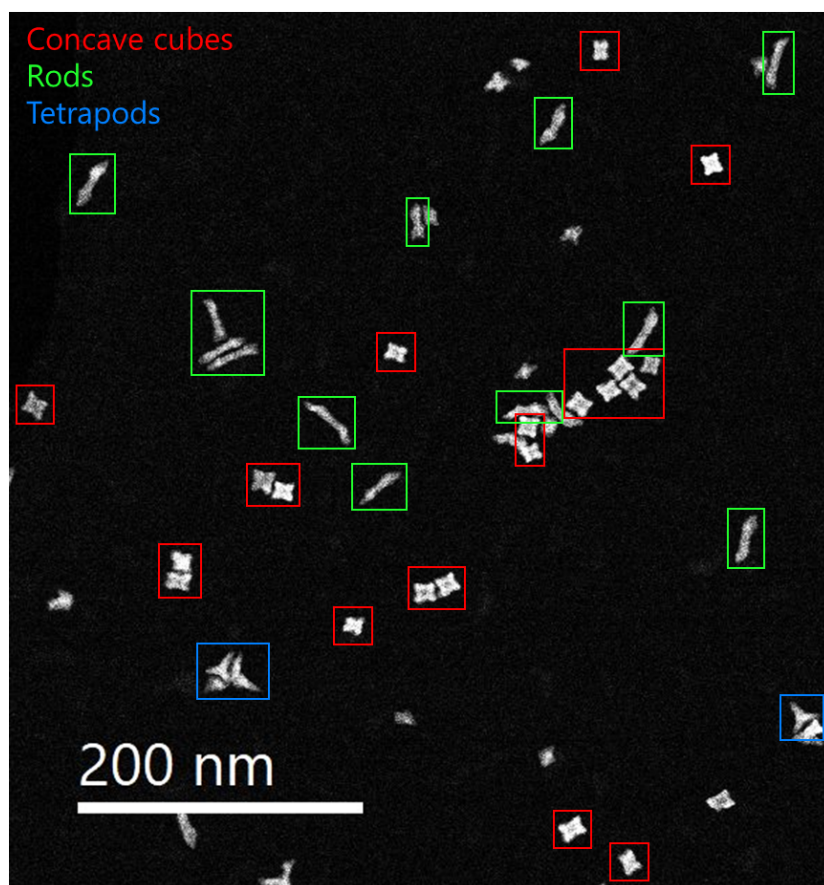
Fig. S1 Low-magnification STEM image of as-grown nanoparticles.
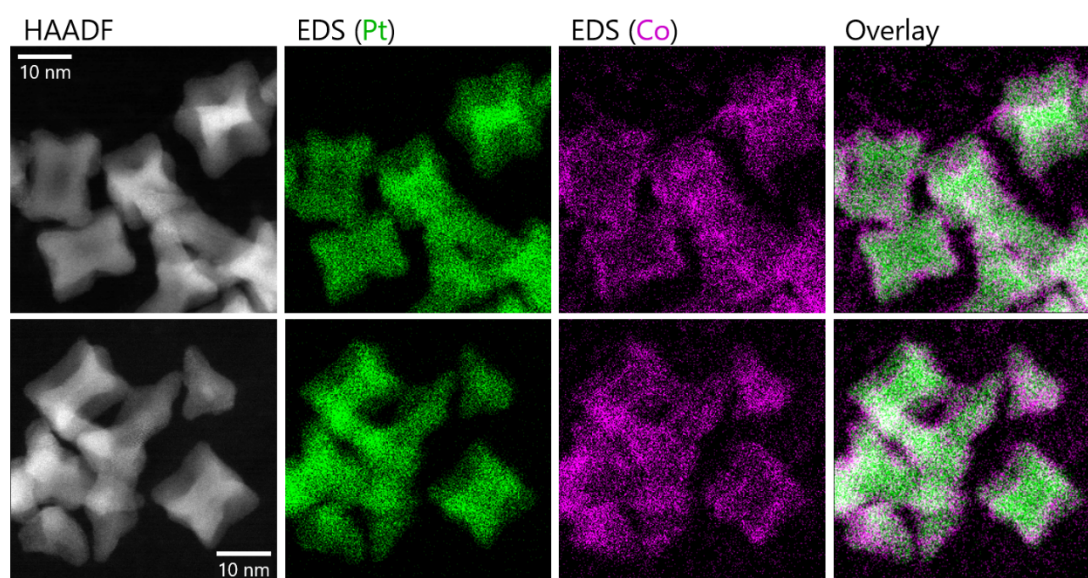
Fig. S2 EDS maps of several as-grown nanoparticles.
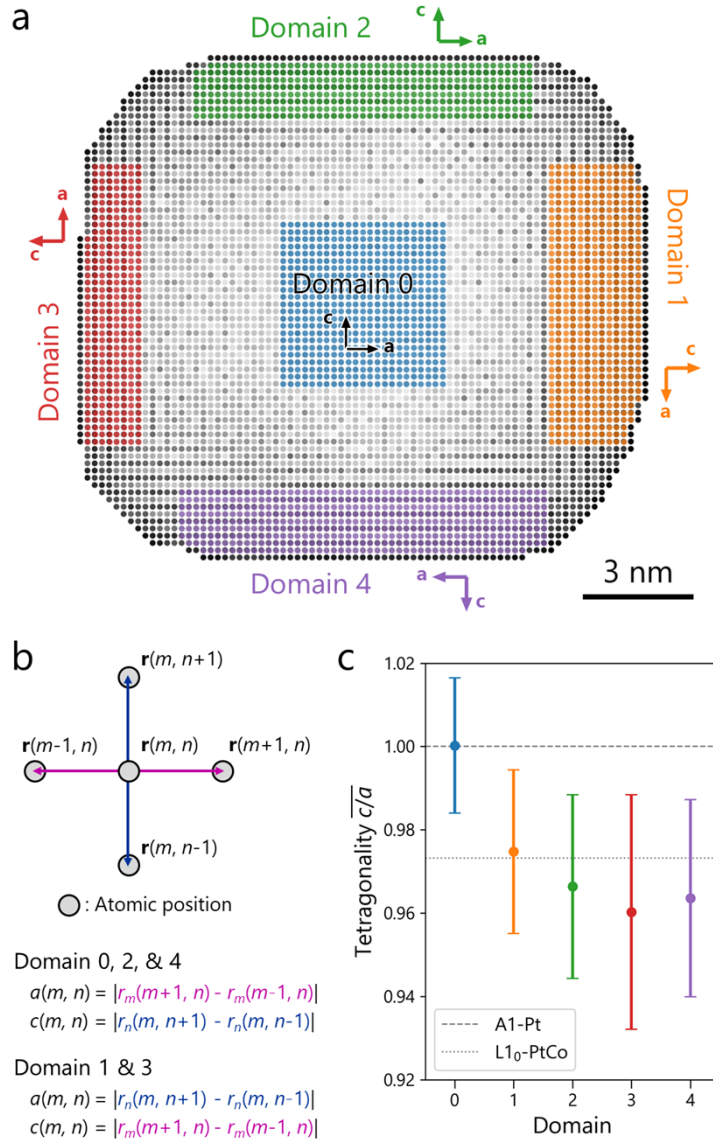
Fig. S3 Atomic distance analysis for the investigation of the tetragonality in L1$_0$ domains. **(a)** Detected atomic positions and the domain configurations. Domain 0 is the reference area for the image distortion correction. Domains 1–4 correspond to the area of the L1$_0$ domains. The brightness of each point corresponds to the image intensity. **(b)** A schematic illustration of the analysis. The vector $\mathbf{r}(m, n)$ means the atomic position $\mathbf{r} = (x, y)$ with the pair of integer index (m, n). **(c)** The tetragonality plot for each domain. The error bars correspond to single standard deviations. The horizontal lines were drawn according to the reported values[7].
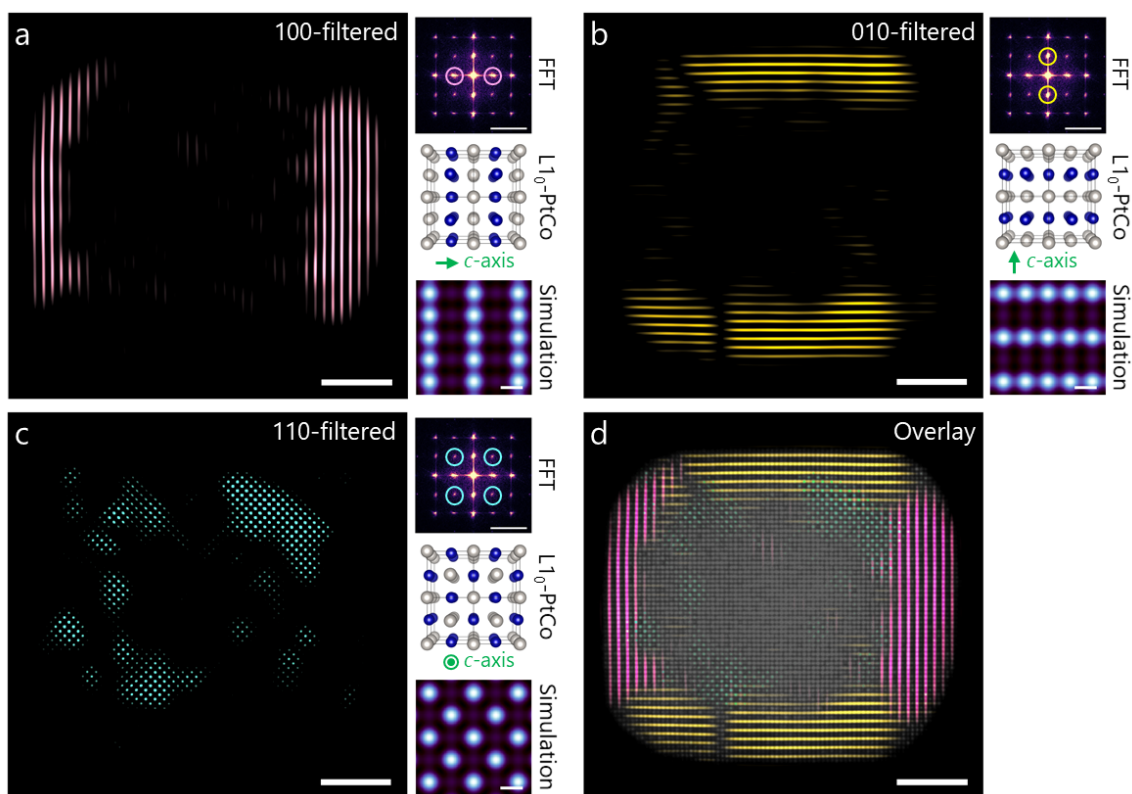
Fig. S4 Fourier filtered images of Main Fig. 2c for **(a)** 100 **(b)** 010 **(c)** 110 spots in the fast Fourier transformed (FFT) patterns, and **(d)** the overlay of the filtered images. The scale bars are 3 nm in the filtered images, $(200 \text{ pm})^{-1}$ in the FFT patterns, and 200 pm in the simulation, respectively.
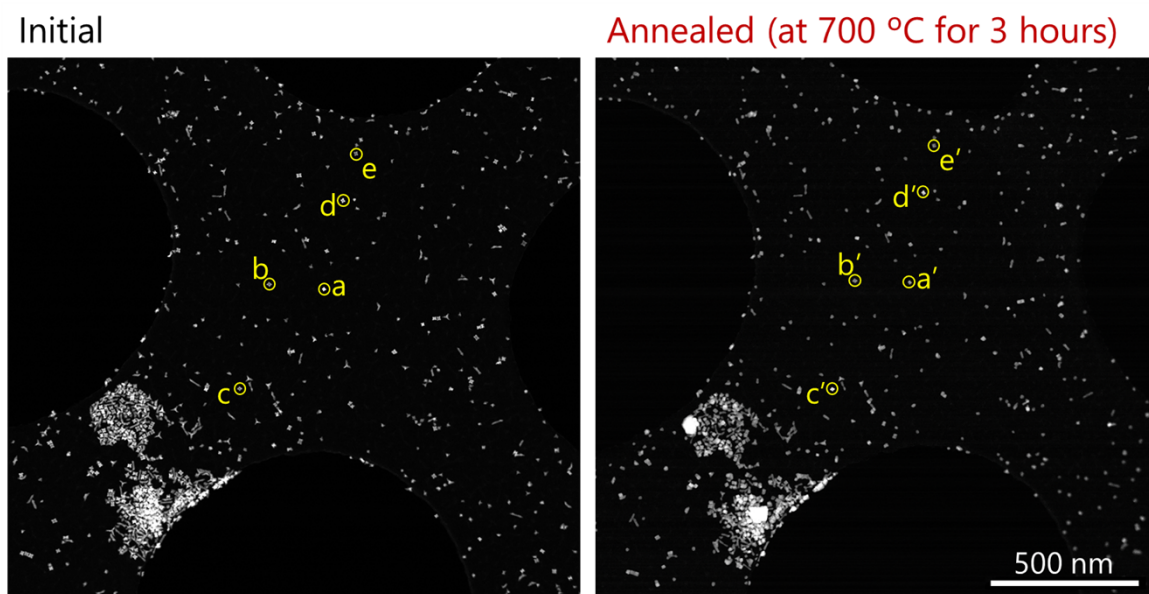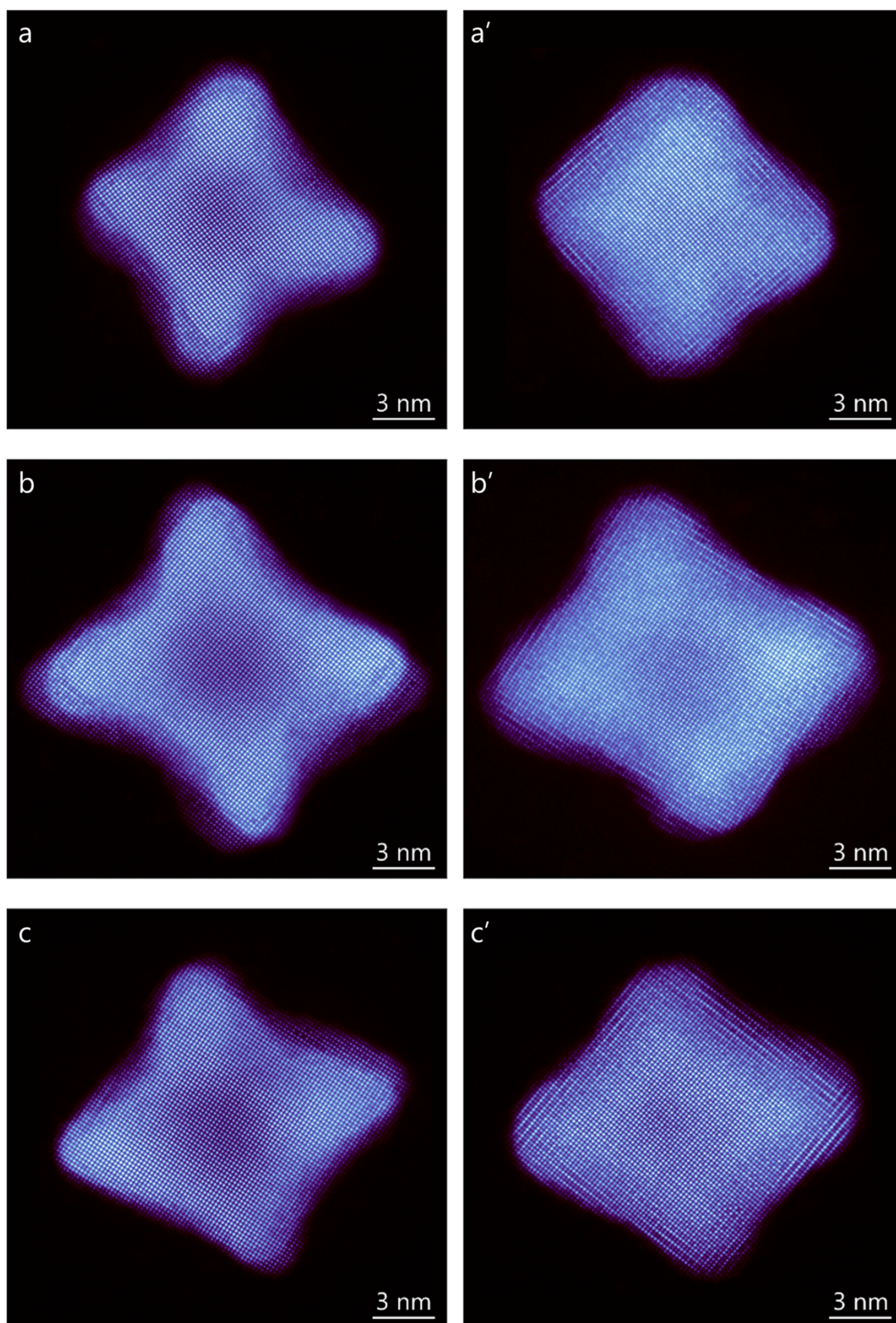

Fig. S5 Atomic-resolution HAADF images of the particles before (left-side) and after (right-side) being annealed at 700°C for 3 hours.

Initial   Annealed

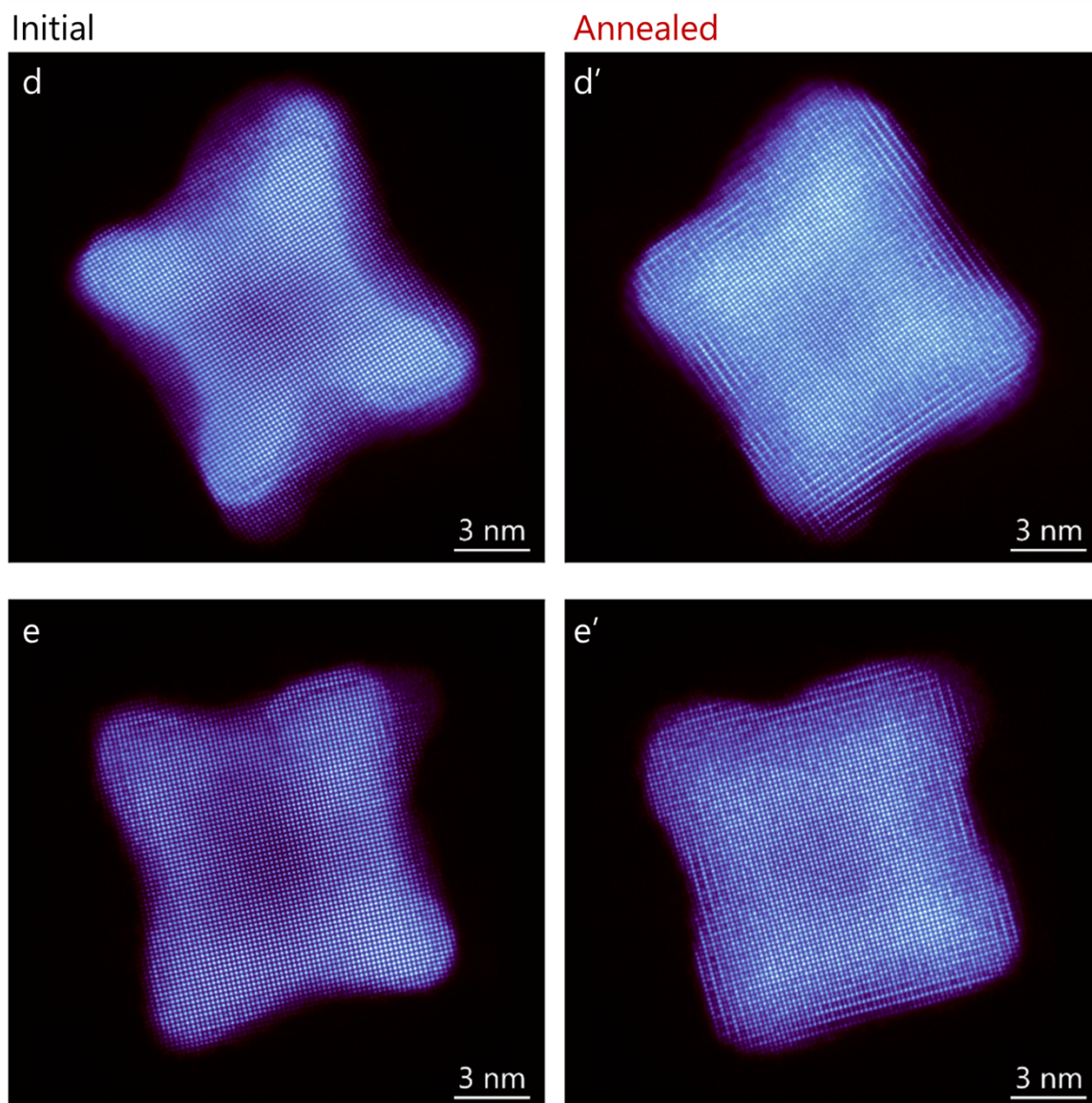

a   a'
3 nm   3 nm

b   b'
3 nm   3 nm

c   c'
3 nm   3 nm

(Fig. S6, continuing)

Fig. S6 Atomic-resolution HAADF images of the particles before **(a–e)** and after **(a'–e')** *ex-situ* annealing at 700°C for 3 hours. The particle alphabets correspond to the ones in Fig. S5.
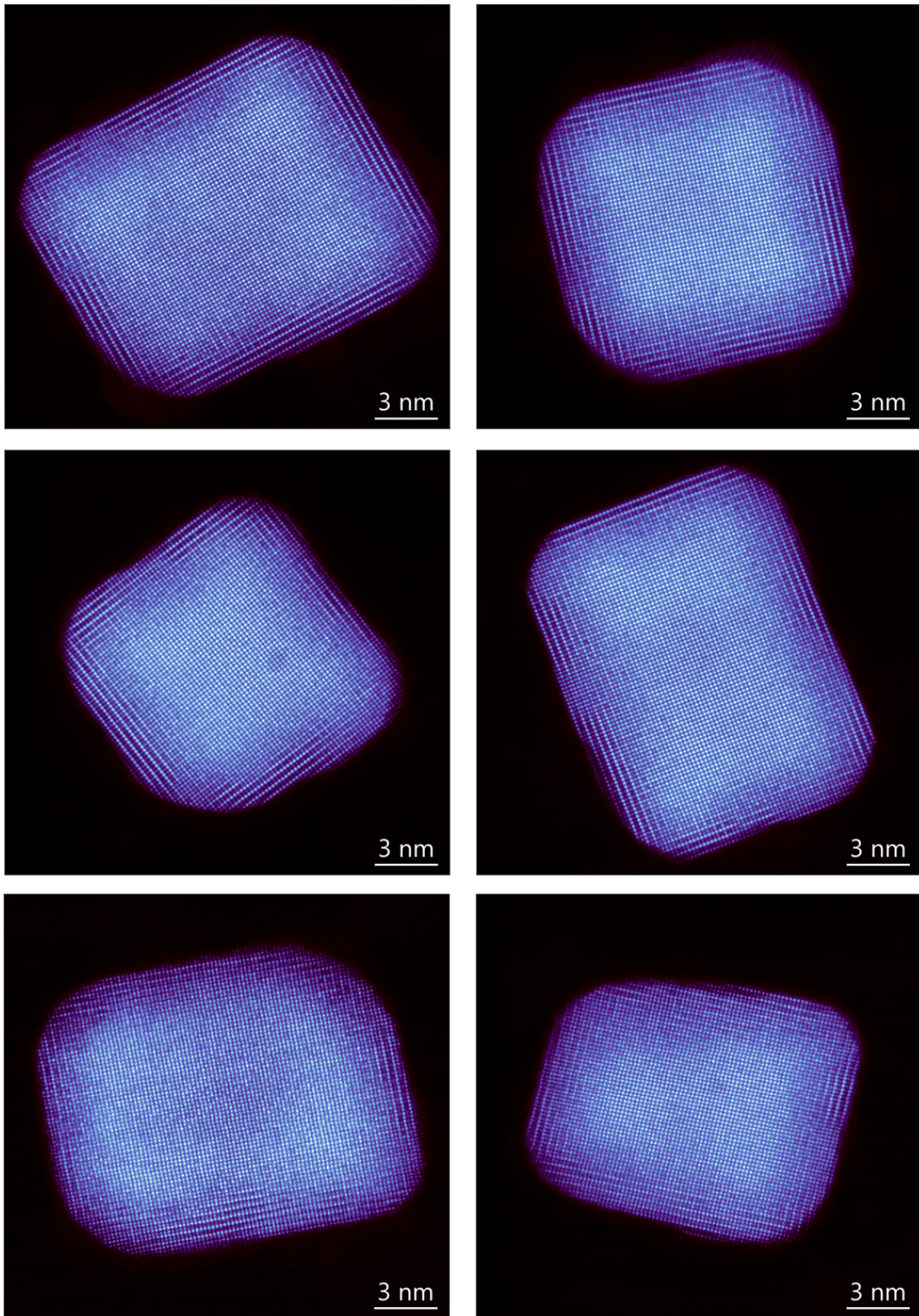
Fig. S7 Atomic-resolution HAADF images of the particles after *ex-situ* annealing at 700°C for 3 hours. Note that the bottom two images are recorded for only a single frame with a scan speed of 15 μs/pixel.
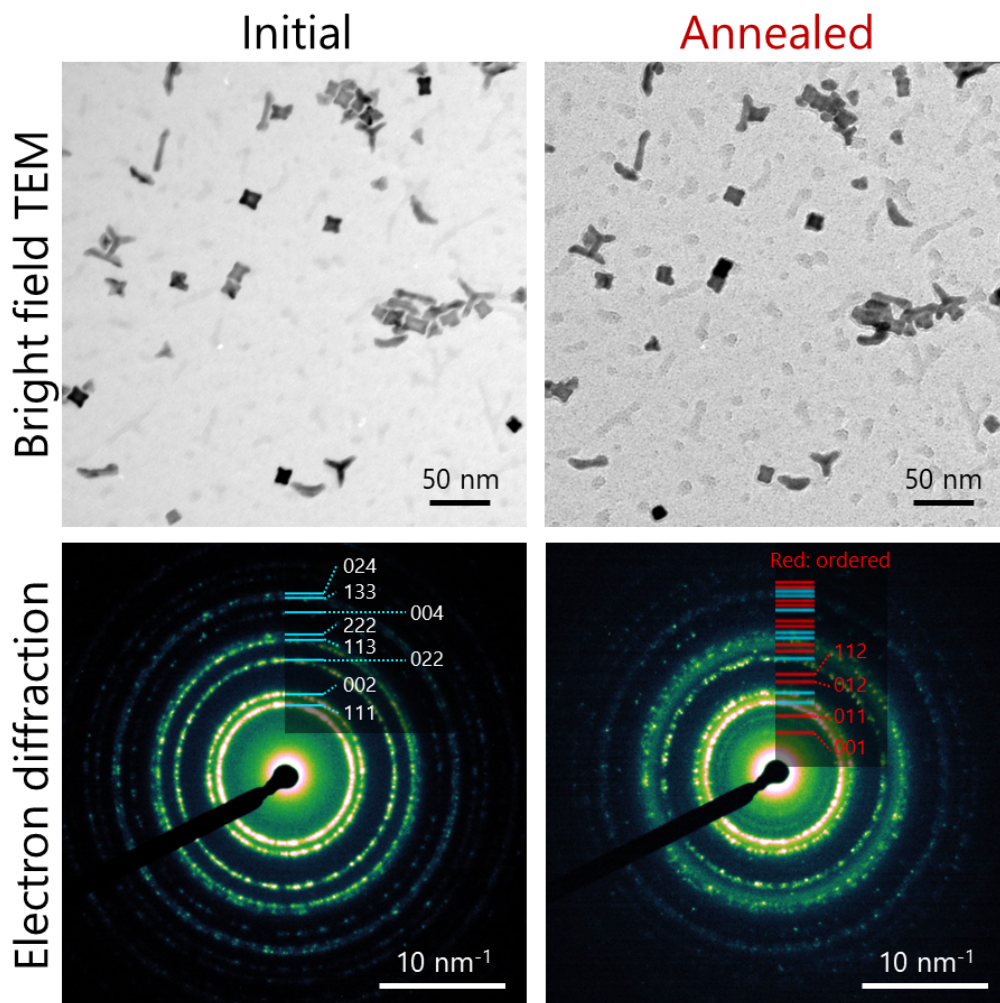
Fig. S8 TEM bright-field images and corresponding electron diffraction patterns, observed before and after *in-situ* heating experiments (annealed at 700°C for 3 hours). Note that the diffraction lines were calculated without considering the ring splitting due to the tetragonal structure of $L1_0$.
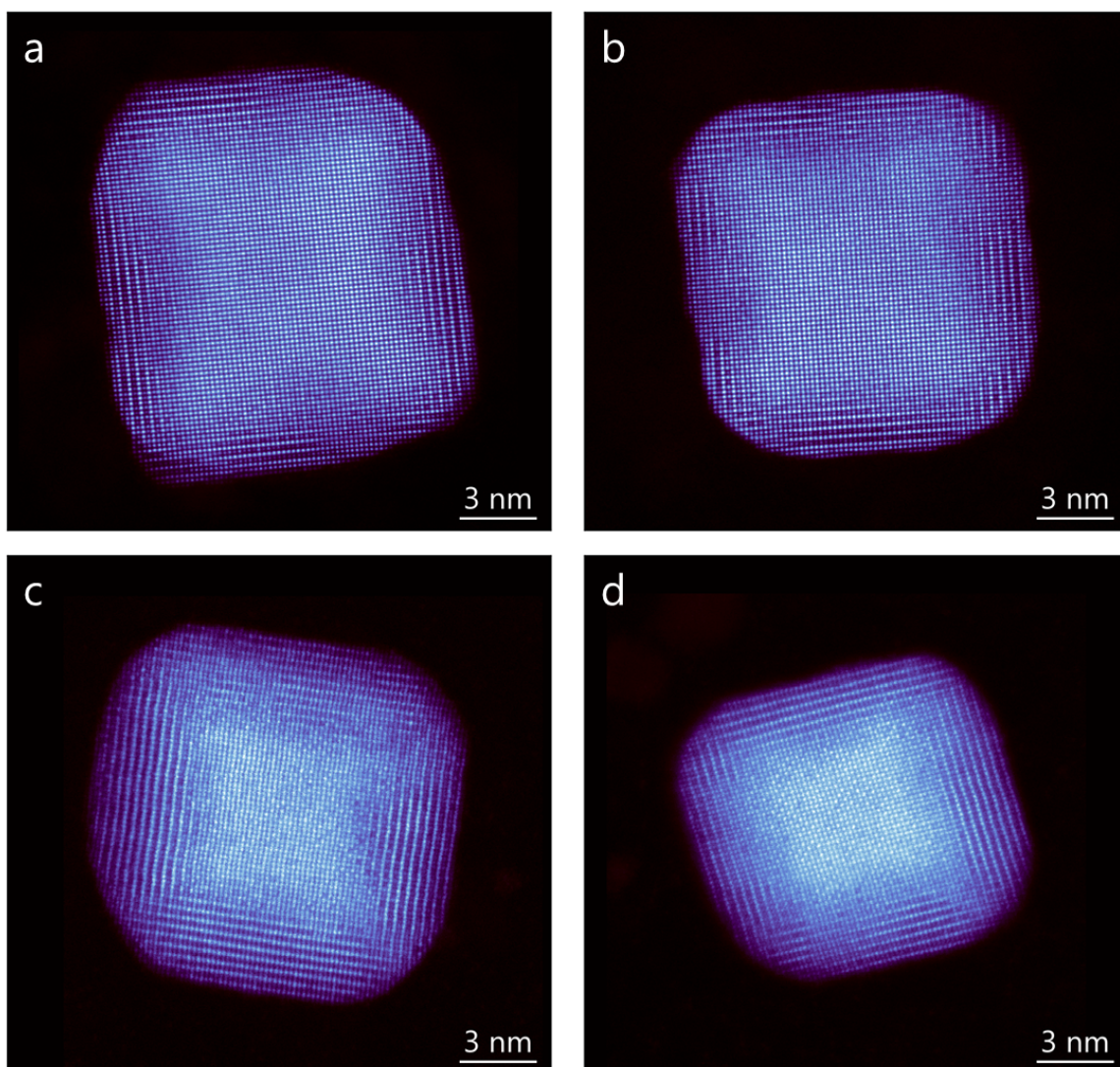
Fig. S9   Atomic-resolution HAADF images of the particles after being annealed at 700°C for 3 hours in *in-situ* experiments in the conventional TEM. The particles in **a** and **b** were observed from the sample after *in-situ* electron diffraction experiments (Fig. S8). The particles in **c** and **d** are observed from the sample after another *in-situ* experiment, where the heating condition is set to be the same. Note that the images in **c** and **d** are recorded for only a single frame with a scan speed of 15 µs/pixel.
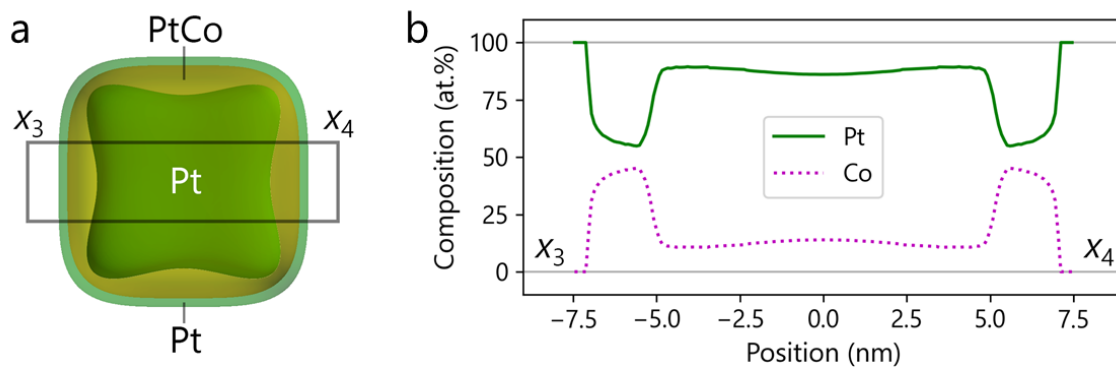
Fig. S10 Three-dimensional volumetric model of a Pt@PtCo@Pt core–shell–shell nanoparticle **(a)** and the composition line profile of the volumetric model **(b)** to be compared with Main Fig. 3c.
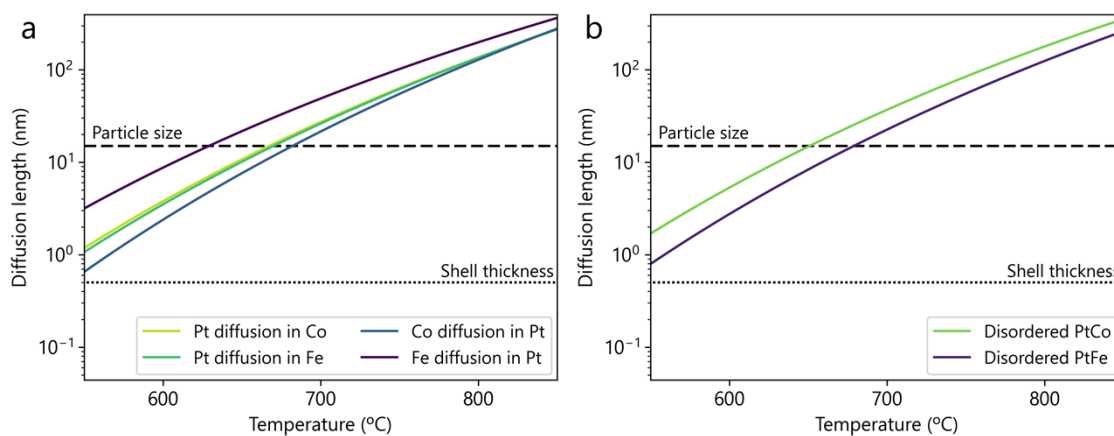

Fig. S11 Diffusion lengths of Pt, Co, and Fe as a function of temperature. **(a)** Tracer diffusion. **(b)** Interdiffusion in disordered alloys. Note that the plotting ranges are set to be the same as in Fig. 4 in the main text.

References

1   S.-I. Choi, R. Choi, S. W. Han and J. T. Park, *Chem. - A Eur. J.*, 2011, **17**, 12280–12284.

2   K. Aso, K. Shigematsu, T. Yamamoto, and S. Matsumura, *Microscopy*, 2016, **65**, 391–399.

3   K. Aso, J. Maebe, X. Q. Tran, T. Yamamoto, Y. Oshima and S. Matsumura, *ACS Nano*, 2021, **15**, 12077–12085.

4   K. Momma and F. Izumi, *J. Appl. Crystallogr.*, 2011, **44**, 1272–1276.

5   Y. Makinen, L. Azzari and A. Foi, in *2019 IEEE International Conference on Image Processing (ICIP)*, IEEE, 2019, pp. 185–189.

6   L. Azzari and A. Foi, *IEEE Signal Process. Lett.*, 2016, **23**, 1086–1090.

7   P. Andreazza, V. Pierron-Bohnes, F. Tournus, C. Andreazza-Vignolle and V. Dupuis, *Surf. Sci. Rep.*, 2015, **70**, 188–258.

8   A. De Backer, K. H. W. van den Bos, W. Van den Broek, J. Sijbers and S. Van Aert, *Ultramicroscopy*, 2016, **171**, 104–116.

9   S. Fujinaka, Y. Sato, R. Teranishi and K. Kaneko, *J. Mater. Sci.*, 2020, **55**, 8123–8133.

10   A. Kushida, K. Tanaka and H. Numakura, *Mater. Trans.*, 2003, **44**, 59–62.

11   Y. Nos, T. Ikeda, H. Nakajima and H. Numakura, *Mater. Trans.*, 2003, **44**, 34–39.

12   G. Neumann and C. Tuijn, *Self-diffusion and impurity diffusion in pure metals: Handbook of experimental data*, 2009.

13   Y. Iijima, O. Taguchi and K. Hirano, *Trans. Japan Inst. Met.*, 1980, **21**, 366–374.